科学通报 2017 年 第 62 卷 第 20 期: 2279 ~ 2286
专题: 二维材料与器件(Ⅰ) 论 文
《中国科学》杂志社
SCIENCE CHINA PRESS

化学气相沉积法在Cu-Ni合金衬底上生长多层六方氮化硼

杨鹏[1,2], 吴天如[2], 王浩敏[2], 卢光远[2], 邓联文[1*], 黄生祥[1]

1. 中南大学物理与电子学院, 长沙 410083;
2. 中国科学院上海微系统与信息技术研究所, 信息功能材料国家重点实验室, 上海 200050
* 联系人, E-mail: dlw626@163.com

2016-11-24 收稿, 2017-01-06 修回, 2017-01-18 接受, 2017-05-17 网络版发表
国家自然科学基金(11304337)资助

摘要 六方氮化硼(h-BN)由于其原子级平整的表面和宽带隙性质使其成为众多二维半导体材料理想的绝缘衬底. 通常情况下通过化学气相沉积法在金属表面生长的h-BN表现出明显的自限生长效应, 仅得到单原子层的h-BN. 采用单原子层的h-BN作为其他二维半导体材料的基底对其下方衬底表面悬挂键及电荷的屏蔽效果有限, 多层h-BN可以提高屏蔽效果. 本文通过化学气相沉积法, 采用生长-刻蚀-再生长的方案在铜镍合金衬底上成功制备得到多层h-BN晶畴, 刻蚀过程使铜镍合金重新漏出, 显著提高了下一阶段生长过程中多层h-BN的外延生长速率, 通过该方案得到三角形状的多层h-BN晶畴尺寸可达10~20 μm. 同时, 使用扫描电子显微镜、X射线光电子能谱、拉曼光谱、透射电子显微镜等一系列测试手段对多层h-BN表面形貌、化学成分及微观结构做了进一步表征. 结果表明, h-BN中B 1s和N 1s的电子能谱峰值分别为190.4和397.8 eV, 并且B和N两种元素的含量比为1.02∶1; 多层h-BN的拉曼光谱峰值位移在1365 cm^{-1}, 半高峰宽为18 cm^{-1}; 选区电子衍射结果说明, 多层h-BN层间具有严格的AA′堆垛且每一层h-BN都具有相同的晶格取向. 所有表征结果说明本文所得的多层h-BN单晶具有较好的晶体质量.

关键词 六方氮化硼, 多层, 化学气相沉积, 铜镍合金, 刻蚀, 结构表征

六方氮化硼(h-BN)由于其类似于石墨烯的六方结构及其特殊的物理化学性质成为国内外的研究热点. h-BN为六方层状堆叠结构, 层与层之间以范德华力结合在一起, 每一层面内的B, N原子以sp^2杂化方式形成共价键, 具有较高的机械强度和良好的化学稳定性[1,2]. h-BN独特的结构使其具有众多优良的物理化学性质. h-BN和石墨烯的晶格常数失配比只有1.6%, 两者在层间堆叠时可形成周期性超晶格结构并呈现出特殊的电子性质, 如优良的热传导、界面电子重构等[3~6]; 通过形成平面异质结有望打开石墨烯的带隙并对其大小进行调控, 从而得到高开关比的石墨烯场效应晶体管[7,8]. 此外, h-BN具有原子级的平整度、表面无悬挂键、宽带隙(~6 eV)、良好的热导性等特点, 使其非常适合用作其他二维材料(如石墨烯, MoS_2, WSe_2等)的衬底. 在室温下测得石墨烯在h-BN衬底上的载流子迁移率高达20000 $cm^2/(V\ s)$, 比SiO_2/Si作为石墨烯衬底时高出一个数量级[2,4,9,10]. 另外, 化学性质稳定的h-BN对可见光几乎不产生吸收, 但对波长为215 nm的紫外线会产生较强吸收, 有望用于紫外线发射器设计[11].

制备h-BN的方法有分子束外延生长(MBE)、机械剥离、液相剥离及化学气相沉积(chemical vapor deposition, CVD)等[12~15]. MBE法生长h-BN虽然能在一定程度上得到高质量的h-BN薄膜, 但成本较高[12].

引用格式: 杨鹏, 吴天如, 王浩敏, 等. 化学气相沉积法在 Cu-Ni 合金衬底上生长多层六方氮化硼. 科学通报, 2017, 62: 2279–2286
Yang P, Wu T R, Wang H M, et al. Synthesis of multilayer hexagonal boron nitride on Cu-Ni alloy by chemical vapor deposition (in Chinese). Chin Sci Bull, 2017, 62: 2279–2286, doi: 10.1360/N972016-01311

机械剥离法也能得到较高质量的单层或多层氮化硼单晶, 但存在尺寸太小、层数不可控及实验重复性差等缺点, 难以使h-BN满足规模应用要求[13]. 目前采用CVD法在金属衬底表面生长h-BN时, 易出现明显的自限生长效应, 即单原子层h-BN很容易铺满整个金属衬底表面, 将阻碍金属衬底对反应前驱体的催化分解, 从而抑制多层h-BN的形核及外延生长. 据报道, 在无金属催化作用下h-BN的生长速率会减小2个数量级[14,16].

针对CVD法在金属衬底表面生长多层h-BN存在的问题, 本文采用氨硼烷作为反应源, 通过设计和优化刻蚀-生长-再刻蚀的工艺条件, 在Cu-Ni合金衬底上成功制备多层取向一致且厚度均一的h-BN单晶, 且尺寸比直接在铜箔上得到的h-BN多层材料的尺寸大1个数量级[14]. 引入刻蚀工艺将部分区域的单层h-BN刻蚀后使该区域的金属衬底重新外露, 可以保持再次生长过程中金属对反应基元的较高催化效率, 有利于多层h-BN的形核与外延生长. 本文还借助场发射扫描电子显微镜(FESEM)、X射线光电子能谱(XPS)、拉曼光谱、透射电子显微镜(TEM)等测试分析手段, 对制备的h-BN试样的形貌和微观结构进行了表征分析.

1 实验

(ⅰ) 铜镍合金衬底制备. 将尺寸为7 cm×7 cm的铜箔(25 μm, 99.8%, Alfa-Aesar, 中国)先通过电化学抛光以减少铜箔表面的粗糙度, 电化学抛光溶液由500 mL水、250 mL乙醇、250 mL磷酸、50 mL异丙醇、5 g尿素组成. 将铜箔连接电源的阳极并通以10 A的恒定电流, 通过90 s的电化学抛光后, 铜箔的厚度减小至20 μm. 抛光后的铜箔在氩气、氢气比为400∶100 sccm (sccm: 标准mL/min)的常压气氛下, 以15℃/min速率升温至1050℃, 退火2 h, 退火过程将去除抛光过程中引入的杂质并进一步增加铜箔表面平整度. 另配制1 L含镍电镀液, 溶液由280 g六水合硫酸镍、8 g六水合氯化镍、30 g硼酸、4 g氟化钠组成, 控制电镀液的pH在4.0~4.5. 经退火后的铜箔连接电源阴极进行电镀镍, 阳极与镍板连接, 调节电源电流密度为0.01 A/cm^2, Ni在铜箔上的沉积速率约为200 nm/min. 本文采用$Cu_{80}Ni_{20}$(摩尔分数)双层衬底, 电镀镍至铜箔的时间为20 min.

(ⅱ) 多层h-BN的生长机制. 本文采用生长-刻蚀-再生长的化学气相沉积工艺, 在低压下生长多层单一取向的多层六方氮化硼单晶; 实验装置示意图如图1(a)所示, 生长源氨硼烷(97%, Aladdin, 中国)和铜镍双层衬底分别置于多温区的炉体中, 且保证对不同区域温度的精确控制. 首先将铜镍双层衬底放入石英管且置于双温区管式炉(OTF-1200X-Ⅱ, 合肥科晶材料技术有限公司, 中国), 在压强为5 kPa、氩气氢气混合气体(Ar 150 sccm, H_2 50 sccm)气氛下退火1 h后, 铜镍完全互熔形成合金; 接下来对氨硼烷升温, 先从室温快速升温到75℃, 时间为10 min; 再从75℃缓慢升温到85℃, 时间为1 h; 氨硼烷在75~85℃的温度区间受热分解, 随着氩气、氢气载气(气体流量分别为15, 100 sccm)流向铜镍合金衬底, 在高温区进一步分解并最终在铜镍合金表面形成h-BN[14,17~22]. h-BN生长示意图如图1(b)所示, 在通氨硼烷生长1 h结束后, 单原子层h-BN铺满整个铜镍合金衬底表面, 伴随有少量尺寸很小的多层h-BN; 当停止氨硼烷供应, 在无生长源的条件下, 部分单层h-BN的晶界处会被刻蚀, 重新暴露的铜镍合金使其保持对反应基元的催化效率, 促进多层h-BN的形核并提高其外延生长速率; 随后恢复氨硼烷的供给, 再次生长过程会出现多层h-BN晶畴尺寸的显著增大.

(ⅲ) 多层h-BN的PMMA转移. 在铜镍合金衬底上生长好h-BN后, 旋涂一层厚度均匀的聚甲基丙烯酸甲酯(PMMA); 然后浸入3 mol/L的$FeCl_3$溶液中对铜镍合金进行化学腐蚀; 待Cu-Ni合金完全腐蚀完毕后, 将h-BN/PMMA用去离子水漂洗并转移至含90 nm厚度SiO_2氧化层的Si片上; 将PMMA/h-BN/SiO_2/Si置于丙酮溶液中加热, 溶解PMMA并用去离子水冲洗, 最后在300℃温度下退火处理h-BN/SiO_2/Si, 进一步除去残留的PMMA.

(ⅳ) 透射电子显微镜试样的聚焦离子束技术(FIB)制备. 使用FIB对多层h-BN切片, 首先通过电子束扫描样品表面找到多层氮化硼区域; 为避免在使用Ga离子束切片过程中对h-BN破坏, 依次沉积Pt, W保护层(总厚度约为300 nm); 然后用30 kV的Ga离子束对已沉积保护层的多层h-BN切片. 切片完成后减小Ga离子束的加速电压, 先用5 kV的Ga离子束流对样品截面粗略修饰, 然后在2 kV的Ga离子束流下对切得的薄片进一步减薄, 为保证透射电子显微镜的高能电子能穿过薄片并清晰成像, FIB切得的薄片厚度要小于100 nm.

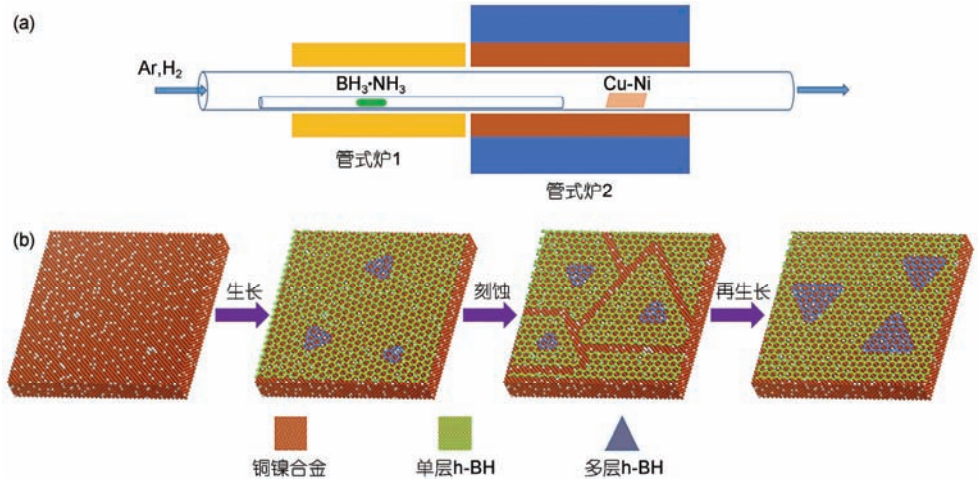

图 1 (网络版彩色)(a) 生长设备示意图; (b) 多层h-BN生长-刻蚀-再生长过程示意图

Figure 1 (Color online) (a) Schematic illustration of the CVD system for multilayer h-BN growth; (b) schematics showing the growth-etching-regrowth process of multilayer h-BN on Cu-Ni alloy

2 结果与讨论

2.1 生长时间及刻蚀工艺对h-BN的影响

据报道，在一定范围内随铜镍合金中镍含量的增加，单层h-BN的形核密度逐渐减小[23]. 通过实验方案优化，拟采用$Cu_{80}Ni_{20}$合金作为生长h-BN的衬底. 生长时间为1 h(图2(a))的试样形貌如图2(d)所示，可见在铜镍合金衬底上长满了单原子层h-BN及少量多层h-BN. 由于硼、氮两种元素几乎不溶于铜镍合金中，表现出明显的自限生长效应，仅得到单层及尺寸很小的多层h-BN晶畴，这与直接在铜箔上生长h-BN的情况类似[14]. 为了使铜镍合金重新露出保持对反应基元的催化效率，停止对氨硼烷源加热(图2(b))，在无生长源供应下部分单层h-BN被刻蚀，h-BN形貌如图2(e)所示，箭头所指区域为被刻蚀部分. 通过实验发现，当增加氢气分压或增加铜镍合金中镍的含量时，刻蚀现象变得更加明显，与前期的研究结果一致[23,24]. 为得到更大尺寸的多层h-BN，重复上述生

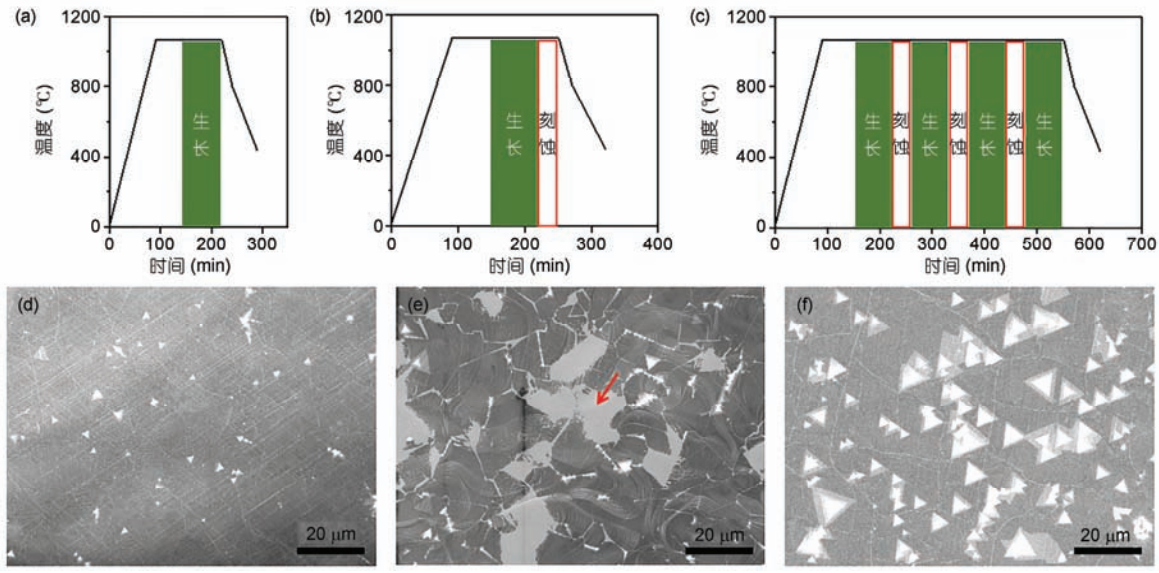

图 2 (网络版彩色)(a)~(c) 生长-刻蚀-再生长过程管式炉温度随时间的变化; (d)~(f) 多层h-BN的SEM形貌(生长参数条件分别对应(a)~(c))

Figure 2 (Color online) (a)–(c) Time dependence of experimental parameters for growth-etching-regrowth h-BN grains; (d)–(f) tipical SEM images of multilayer h-BN corresponding to the growth parameters of (a)–(c), respectively

长-刻蚀过程, 工艺参数如图2(c)所示, 对氨硼烷加热时间为4 h, 多层h-BN的形核密度及尺寸显著增加并呈现为三角形状, 其边长尺寸达10~20 μm(图2(f)). 通过生长-刻蚀-再生长过程, 多层h-BN的尺寸显著增加. 在停止对氨硼烷加热过程中, 部分单原子层h-BN被刻蚀使Cu-Ni合金衬底重新露出, 对下一阶段多层h-BN的形核及外延生长起催化作用.

2.2 不同层数的h-BN生长

在生长h-BN的实验方案中, 可同时得到单原子层及不同层数的多层h-BN. 图3(a)为单原子层h-BN单晶, 前期研究表明通过CVD法在铜镍合金上生长得到的h-BN具有较高质量[23]. 经生长-刻蚀-再生长可以得到系列不同层数的h-BN(图3(b)~(d)), 每层h-BN都为三角形状且具有相同取向. 关于h-BN是直接还是间接带隙半导体目前还存在争议[25~27]. 二维半导体材料的带隙特性不仅与层间的堆垛方式、掺杂及缺陷有关, 还与其层数有关[28], 本文通过CVD法得到不同层数的h-BN将有可能进一步揭示h-BN的带隙特性.

2.3 多层h-BN的XPS及拉曼光谱表征

X射线光电子能谱不仅可以对元素的种类及所处的化学环境(如价态、化学键种类等)进行定性分析, 还可以对各种不同元素的含量进行定量分析. 对铜镍合金衬底上的多层h-BN进行XPS表征如图4(a)所示, 能明显检测到Cu, Ni, O, N, C及B等元素, 其中C和O可能是由于h-BN样品暴漏在空气中引入, 右上方插图为XPS探测区域多层h-BN的SEM形貌. 图4(b), (c)对B, N元素进一步分析可以看出, B和N元素各自的1s内层电子的结合能谱都具有完美对称峰型, 其峰值分别位于190.4和397.8 eV, 表明B, N原子以sp^2杂化方式形成化学键[29,30]. 此外, 通过计算B, N能谱峰的积分面积可得到两种元素含量比为1.02:1, 接近于h-BN的化学计量比.

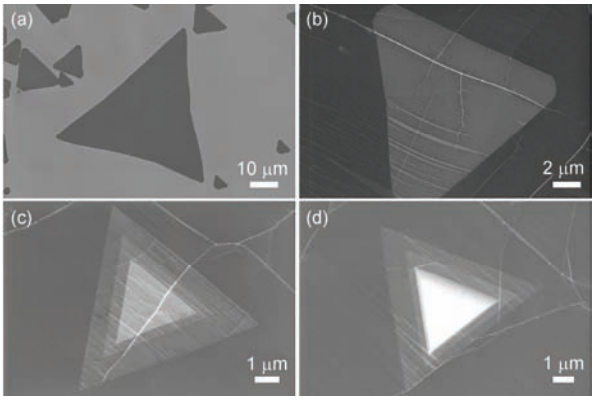

图 3 不同层数的h-BN. (a) 单原子层h-BN; (b)~(d) 不同层数的多层h-BN

Figure 3 Different layers of h-BN. (a) Monolayer h-BN; (b)–(d) different layers of multilayer h-BN

拉曼光谱能快速、高效率、无损表征h-BN的晶体质量. 通过研究拉曼光谱谱线的形状、半高峰宽和峰位等可以分析h-BN结晶质量优劣. 图4(d)为h-BN转移至90 nm厚SiO_2/Si衬底后的光学显微镜形貌, 转移后的多层h-BN较好地保留了其原来的三角形状. 通过拉曼光谱对多层h-BN区域进一步表征(图4(e)), 拉曼光谱峰值为1365 cm^{-1}, 此峰值由h-BN的E_{2g}对称振动模产生, 与单层h-BN相比发生6 cm^{-1}红移[23], 可能原因是在退火过程中单层h-BN受到衬底较大的拉伸应力所致, 通过机械剥离的多层h-BN与单层的相比, 其拉曼峰位移也出现类似规律[13]; 多层h-BN的半高峰宽为18 cm^{-1}, 且峰型具有良好对称性, 说明所得到的多层h-BN具有较高结晶质量[2,13].

2.4 多层h-BN的TEM表征

将铜镍合金衬底上的多层h-BN转移至带有碳膜的铜网上并使用TEM对其结构进行表征. 图5(a)为低倍下多层h-BN的TEM图, 图5(a)中的B点区域的高分辨TEM图如5(b)所示, h-BN呈现良好层状分布, 层间距离为0.33 nm. 对图5(a)中4个不同区域进行电子衍射分析(图5(c)~(f)), 六角点列电子衍射谱具有六次旋转对称轴, 说明多层h-BN以AA′方式进行堆垛[2,31], 4个不同区域的电子衍射都具有同样取向, 进一步说明多层h-BN为单一取向的单晶. 在h-BN中B, N原子均以sp^2杂化方式成键, 其中B原子外层3个电子都已成键, 剩下1个空的p轨道; 而N原子外层的5个电子中有3个与B原子形成共价键, 另有一个孤对电子占据p轨道; 多层h-BN的电子分布及其AA′堆垛方式使其具有良好的化学稳定性. 此外, 对选区电子衍射花样进行标定计算出h-BN的晶格常数为0.25 nm, 与文献[16]报道一致.

为了对所得多层h-BN厚度进一步表征, 采用FIB对图6(a)中的多层h-BN切片, 所得样品在低倍下的TEM图如图6(b)所示, 多层h-BN具有均一厚度. 图6(c)为h-BN截面的高倍TEM图, 多层h-BN的厚度约

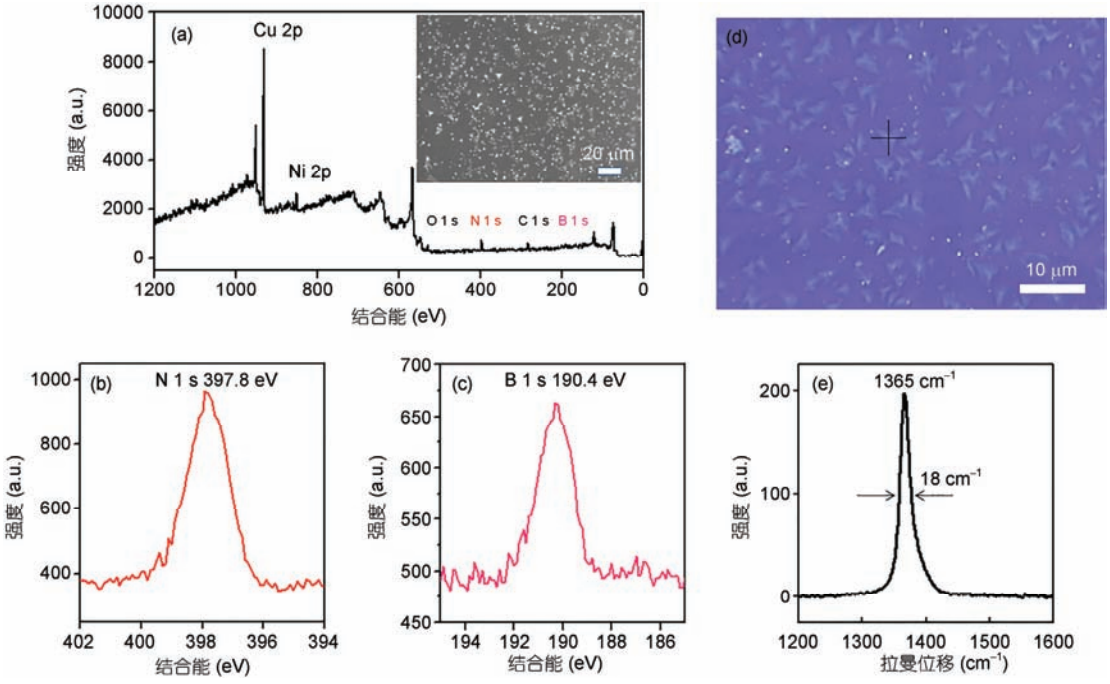

图 4 (网络版彩色)XPS及拉曼光谱表征. (a) 铜镍合金上多层h-BN的不同元素的能谱; N元素(b)和B元素(c)1s层电子对应的峰值; (d) 多层h-BN转移至 90 nm SiO_2/Si上的光学显微镜形貌; (e) 对应于图(d)中十字中心位置的多层h-BN的拉曼光谱

Figure 4 (Color online) Characterization of multilayer h-BN by XPS and Raman spectroscopy. (a) XPS survey of the h-BN on Cu-Ni alloy, the inset image is the XPS detected area corresponding SEM image; N 1s (b) and B 1s (c) XPS spectra, respectively; (d) optical image of multilayer h-BN domains transferred onto 90 nm SiO_2/Si substrate; (e) Raman spectra of multilayer h-BN exited by 514 nm laser

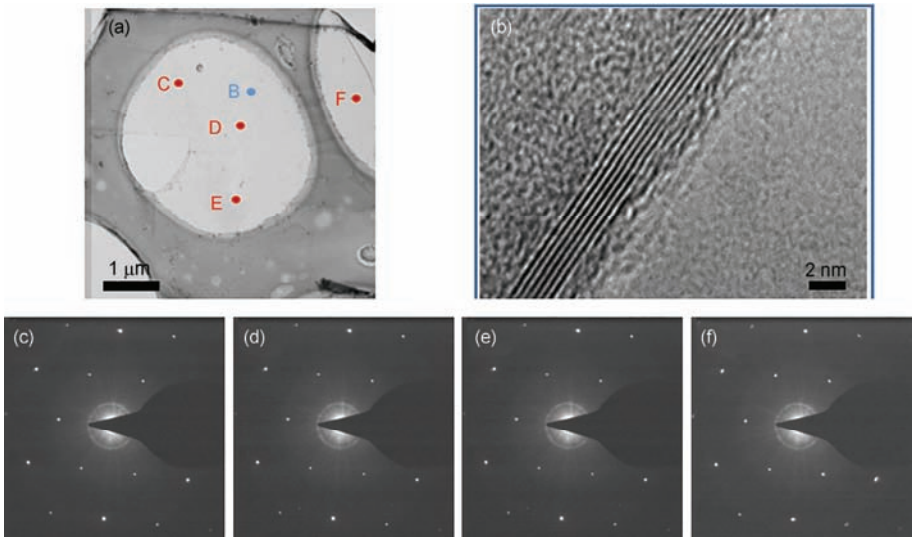

图 5 (网络版彩色)多层h-BN的TEM表征. (a) 多层h-BN在低倍下TEM图; (b) 图(a)中B点折叠区域的高倍TEM图; (c)~(f) 选区电子衍射图分别对应图(a)中的C, D, E, F位置. 衍射光阑直径为 180 nm

Figure 5 (Color online) Characterizations of multilayer h-BN by TEM. (a) Low-magnification TEM images of a multilayer h-BN domain; (b) cross-sectional TEM images of h-BN domain from folded area in (a); (c)–(f) SAED patterns taken from four representative regions indicated in (a), the diameter of diffraction spot is 180 nm

为10 nm, 对其中的某一个区域放大后如图6(d)所示, 多层h-BN呈现出良好的层状分布并未产生错层现象, 单原子层厚度为0.33 nm, 与图5(b)中的厚度一致. 由于切片过程中使用的是2 kV的Ga离子束, 多层h-BN

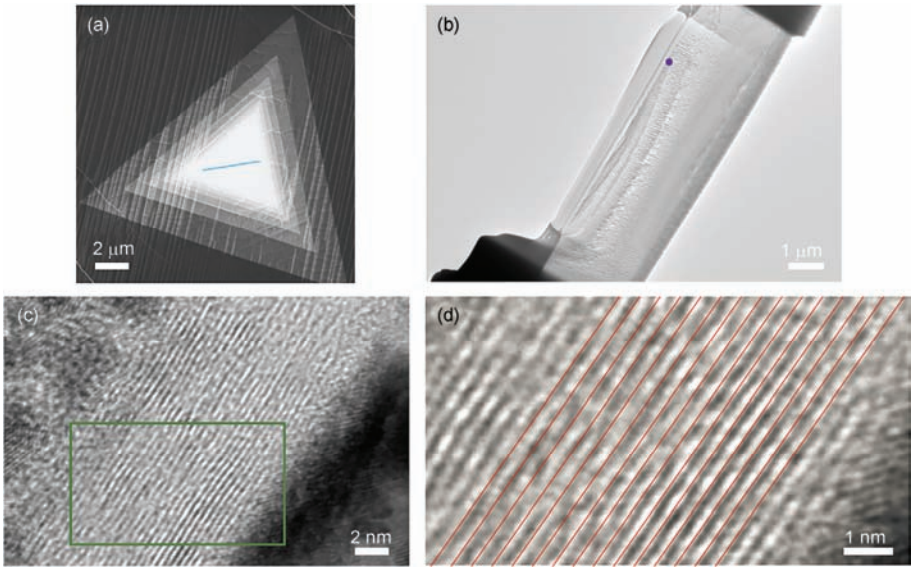

图 6 (网络版彩色)多层h-BN截面表征. (a) 多层h-BN切片前通过SEM观察到的形貌; (b) 选取(a)中对应区域采用FIB切片所得样品的低倍TEM图; (c) 对应图(b)圆点区高倍TEM图, 多层h-BN的厚度约为 10 nm, 单层h-BN的厚度为 0.35 nm; (d) h-BN呈现较好的层状分布且无错层现象

Figure 6 (Color online) Cross-sectional TEM characterizations of multilayer h-BN. (a) SEM image of multilayer h-BN before cutted by FIB; (b) low-magnification TEM image of the cut sample; (c) high-magnification TEM images of multilayer h-BN corresponding to the purple dotted area indicated in (b); (d) enlarged image corresponding to the rectangle area indicated in (c), as illustrated by fitting lines no misfit-layered structure is found

的截面处会不可避免地产生非晶层, 适当降低Ga离子束的加速电压, 非晶层含量有可能进一步减小[32].

3 结论与展望

本文通过生长-刻蚀-再生长的方法在铜镍合金衬底上制备出尺寸达10~20 μm的三角形状、取向一致、厚度均一的多层h-BN单晶, 刻蚀过程使铜镍合金重新露出并显著增加多层h-BN的形核密度和生长速率, 其尺寸比直接在铜箔上面得到的多层h-BN大一个数量级. X射线光电子能谱测得B, N元素1s层电子能谱峰值分别为190.4和397.8 eV, B, N元素含量比为1.02∶1; 拉曼光谱表征测得多层h-BN的峰值位移为1365 cm^{-1}; 进一步的TEM表征确定BN为六方层状结构, 层间距离为0.33 nm, 晶格常数为0.25 nm. 以这种高质量的多层h-BN单晶作为衬底将大幅改善其他二维半导体材料的电学性能, 并有望应用于霍尔器件、场效应晶体管等电学器件领域. 本文生长多层h-BN的方法对其他多层二维材料的制备具有借鉴意义.

致谢 中国科学院上海微系统与信息技术研究所谢红在SEM测试和陈吉在h-BN转移方面提供了帮助, 在此一并致谢.

参考文献

1 Song L, Ci L J, Lu H, et al. Large scale growth and characterization of atomic hexagonal boron nitride layers. Nano Lett, 2010, 10: 3209–3215
2 Kim S M, Hsu A, Park M H, et al. Synthesis of large-area multilayer hexagonal boron nitride for high material performance. Nat Commun, 2015, 6: 8662
3 Yankowitz M, Xue J M, Cormode D, et al. Emergence of superlattice Dirac points in graphene on hexagonal boron nitride. Nat Phys, 2012, 8: 382–386
4 Tang S J, Wang H M, Wang H S, et al. Silane-catalysed fast growth of large single-crystalline graphene on hexagonal boron nitride. Nat Commun, 2015, 6: 6499
5 Wang M, Jang S K, Jang W J, et al. A platform for large-scale graphene electronic-CVD growth of single-layer graphene on CVD-grown hexagonal boron nitride. Adv Mater, 2013, 25: 2746–2752

6 Zhang C H, Zhao S L, Jin C H, et al. Direct growth of large-area graphene and boron nitride heterostructures by a co-segregation method. Nat Commun, 2015, 6: 6519
7 Liu Z, Ma L L, Shi G, et al. In-plane heterostructures of graphene and hexagonal boron nitride with controlled domain sizes. Nat Nanotechnol, 2013, 8: 119–124
8 Levendorf M P, Kim C J, Lola B, et al. Graphene and boron nitride lateral heterostructures for atomically thin circuitry. Nature, 2012, 488: 627–632
9 Dean C R, Young A F, Meric I, et al. Boron nitride substrates for high-quality graphene electronics. Nat Nanotechnol, 2010, 5: 722–726
10 Britnell L, Gorbachev R V, Jalil R, et al. Field-effect tunneling transistor based on vertical graphene heterostructures. Science, 2012, 335: 947–950
11 Watanabe K, Taniguchi T, Niiyama T, et al. Far-ultraviolet plane-emission handheld device based on hexagonal boron nitride. Nat Photon, 2009, 3: 591–594
12 Tonkikh A A, Voloshina E N, Werner P, et al. Structural and electronic properties of epitaxial multilayer h-BN on Ni(111) for spintronics applications. Sci Rep, 2016, 6: 23457
13 Gorbachev R V, Riaz I, Nair R R, et al. Hunting for monolayer boron nitride: Optical and Raman signatures. Small, 2011, 7: 465–468
14 Kim K K, Hsu A, Jia X T, et al. Synthesis of monolayer hexagonal boron nitride on Cu foil using chemical vapor deposition. Nano Lett, 2012, 12: 161–166
15 Tay R Y, Griep M H, Mallick G, et al. Growth of large single-crystalline two-dimensional boron nitride hexagons on electropolished copper. Nano Lett, 2014, 14: 839–846
16 Auwärter W, Kreutz T J, Greber T, et al. XPD and STM investigation of hexagonal boron nitride on Ni(111). Surf Sci, 1999, 429: 229–236
17 Wang L F, Wu B, Chen J S, et al. Monolayer hexagonal boron nitride films with large domain size and clean interface for enhancing the mobility of graphene-based field-effect transistors. Adv Mater, 2014, 26: 1559–1564
18 Kim D P, Moon K T, Kho J G, et al. Synthesis and characterization of poly-(aminoborane) as a new boron nitride precursor. Polym Adv Technol, 1999, 10: 702–712
19 Wolf G, Baumann J, Baitalow F, et al. Calorimetric process monitoring of thermal decomposition of B-N-H compounds. Thermochim Acta, 2000, 343: 19–25
20 Baitalow F, Baumann J, Wolf G, et al. Thermal decomposition of B-N-H compounds investigated by using combined thermoanalytical methods. Thermochim Acta, 2002, 391: 159–168
21 Baumann J, Baitalow F, Wolf G. Thermal decomposition of polymeric aminoborane $(H_2BNH_2)_x$ under hydrogen release. Thermochim Acta, 2005, 430: 9–14
22 Frueh S, Kellett R, Mallery C, et al. Pyrolytic decomposition of ammonia borane to boron nitride. Inorg Chem, 2011, 50: 783–792
23 Lu G Y, Wu T R, Yuan Q H, et al. Synthesis of large single-crystal hexagonal boron nitride grains on Cu-Ni alloy. Nat Commun, 2015, 6: 6160
24 Wu Q K, Park J H, Park S, et al. Single crystalline film of hexagonal boron nitride atomic monolayer by controlling nucleation seeds and domains. Sci Rep, 2016, 5: 16159
25 Watanabe K, Taniguchi T, Kanda H. Direct-bandgap properties and evidence for ultraviolet lasing of hexagonal boron nitride single crystal. Nat Mater, 2004, 3: 404–409
26 Cassabois G, Valvin P, Gil B. Hexagonal boron nitride is an indirect bandgap semiconductor. Nat Photon, 2016, 10: 262–266
27 Edgar J H, Hoffman T B, Clubine B, et al. Characterization of bulk hexagonal boron nitride single crystals grown by the metal flux technique. J Crystal Growth, 2014, 403: 110–113
28 Mak K F, Lee C, Hone J, et al. Atomically thin MoS_2: A new direct-gap semiconductor. Phys Rev Lett, 2010, 105: 136805
29 Shi Y M, Hamsen C, Jia X T, et al. Synthesis of few-layer hexagonal boron nitride thin film by chemical vapor deposition. Nano Lett, 2010, 10: 4134–4139
30 Jang A R, Hong S, Hyun C, et al. Wafer-scale and wrinkle-free epitaxial growth of single-orientated multilayer hexagonal boron nitride on sapphire. Nano Lett, 2016, 16: 3360−3366
31 Pease R S. Crystal structure of boron nitride. Nature, 1950, 165: 722−723
32 Han W, Xiao S Q. Focus ion beam (FIB) and its applications (in Chinese). Mater China, 2013, 32: 12 [韩伟, 肖思群. 聚焦离子束(FIB)及其应用. 中国材料进展, 2013, 32: 12]

Summary for “化学气相沉积法在 Cu-Ni 合金衬底上生长多层六方氮化硼”

Synthesis of multilayer hexagonal boron nitride on Cu-Ni alloy by chemical vapor deposition

YANG Peng[1,2], WU TianRu[2], WANG HaoMin[2], LU GuangYuan[2], DENG LianWen[1*] & HUANG ShengXiang[1]

[1] *School of Physics and Electronics, Central South University, Changsha 410083, China;*
[2] *State Key Laboratory of Functional Materials for Informatics, Shanghai Institute of Microsystem and Information Technology, Chinese Academy of Sciences, Shanghai 200050, China*
* Corresponding author, E-mail: dlw626@163.com

Hexagonal boron nitride (h-BN) is isoelectronic to graphite with an equal number of boron (B) and nitrogen (N) atoms. For bulk h-BN, B and N atoms are bonded together by strong covalent bonds in plane while weak van der Waals force dominates the interaction in-between the layers. h-BN has attractive properties including high mechanical strength, high thermal conductivity, chemical inertness, and excellent electrical insulation. The unique properties of h-BN provide a potential for a wide range of applications as both a structural and electronic material. As h-BN is of a wide band gap, a ultra-smooth surface and a low density of surface charge states, it is always regarded as an ideal substrate for other two dimensional crystals, such as graphene and transition metal dichalcogenides, in electronic applications. Although monolayer single crystal of h-BN has been synthesized on Cu and Cu-Ni alloy foil by chemical vapor deposition (CVD), multilayer h-BN single-crystal has yet not been synthesized successfully. Normally the growth of h-BN by CVD method on metal surface shows an obvious self-limited behavior, and thus h-BN monolayer is always obtained. As a dielectric material for two dimensional semiconductors, the screening effect of monolayer h-BN is limited for electronics. As such, multilayer crystals of h-BN are required to overcome the inextricable difficulty. In this work, we demonstrate an approach to synthesize multilayer single crystal of h-BN on Cu-Ni alloy by using growth-etching-regrowth strategy. In the strategy, growth of the first layer of h-BN was suppressed when H_2 flow is increased and the supply of B-N precursors is reduced. The exposed Cu-Ni alloy significantly improves the growth rate of multilayer h-BN in the next growth process. The morphology of multilayer h-BN samples was characterized by field-emission scanning electron microscope. It is found that multilayer domains of h-BN finally obtained are in triangle with each side up to ~20 μm. X-ray photoemission spectroscopy (XPS) measurement was also done on the h-BN/Cu-Ni sample, the results show that the spectra of B 1s and N 1s were at 190.4 and 397.8 eV, respectively. Raman spectroscopy is used to understand the lattice structure of the h-BN. In the Raman spectrum, only the E_{2g} Raman peak at 1365 cm^{-1} was observed, it indicates that the configuration for B and N atoms is B-N bonding, implying that the hexagonal phase exists in our BN films. The full width at half maximum (FWHM) of Raman peak is 18 cm^{-1}, which is less than the values in earlier literatures and comparable to the single-crystalline bulk h-BN fabricated by high temperature high pressure method. Transmission electron microscope (TEM) and selected area electron diffraction (SAED) were further conducted to characterize the microstructure of the multilayer h-BN domains. Cross-sectional TEM image in a high magnification shows that the interlayer distance of multilayer h-BN is 0.33 nm, and the SAED results indicates that h-BN domains is well-stacked with and AA′ stacking order and each layer of h-BN has the same lattice orientation. All the results show that the multilayer h-BN domains we synthesized are in single-crystalline with high quality.

hexagonal boron nitride, multilayer, chemical vapor deposition, Cu-Ni alloy, etching, characterization

doi: 10.1360/N972016-01311